Available online at www.sciencedirect.com
SCIENCE DIRECT
Journal of Catalysis 234 (2005) 438–450
JOURNAL OF CATALYSIS
www.elsevier.com/locate/jcat

Synthesis of novel core-shell structured WO_3/TiO_2 spheroids and its application in the catalytic oxidation of cyclopentene to glutaraldehyde by aqueous H_2O_2

Xin-Li Yang [a], Wei-Lin Dai [a,*], Changwen Guo [a], Hui Chen [a], Yong Cao [a], Hexing Li [b], Heyong He [a], Kangnian Fan [a,*]

[a] *Department of Chemistry and Shanghai Key Laboratory of Molecular Catalysis and Innovative Materials, Fudan University, Shanghai 200433, PR China*
[b] *Department of Chemistry, Shanghai Normal University, Shanghai 200234, PR China*

Received 19 May 2005; revised 26 June 2005; accepted 29 June 2005

Available online 11 August 2005

Abstract

Novel core-shell structured WO_3/TiO_2 spheroids were synthesized through a conventional incipient wetness impregnation method and systematically characterized by X-ray diffraction, N_2 sorption, scanning electron microscopy, transmission electron microscopy, laser Raman spectroscopy, thermogravimetric and differential thermal analysis, X-ray photoelectron spectroscopy, and NH_3 temperature-programmed desorption. It was found that tungsten species are highly dispersed in the interlayer between the core and the shell layer of the TiO_2 support and that there are interactions between the tungsten species and the TiO_2 support that could provide abundant oxygen defect lattice. It is also found that the as-prepared WO_3/TiO_2 material is highly active as a catalyst for the selective oxidation of cyclopentene to glutaraldehyde with aqueous hydrogen peroxide as the green oxidant. Proper content and high dispersion of tungsten species, the interaction between the tungsten species and the support, as well as the medium strong acidity of the novel WO_3/TiO_2 catalyst all account for this material's high activity.
© 2005 Elsevier Inc. All rights reserved.

Keywords: Titania microsphere; Core-shell structure; Tungsten species; WO_3/TiO_2 catalyst; Cyclopentene; Glutaraldehyde; H_2O_2

1. Introduction

Tungsten oxide-based catalyst has been used in many applications, including selective oxidation of unsaturated compounds [1–4], isomerization and alkylation of hydrocarbons [5], and catalytically selective reduction of nitric oxide with ammonia [6], because their solid acidic and redox properties are thought to change with tungsten coordination. Besides those reactions, this catalyst also has activity for the oxidative cleavage of carbon–carbon double bonds to produce dialdehydes, which are now prepared mainly by ozonization of cycloolefins [7,8] or other synthetic methods [9,10]. Since the first report of glutaraldehyde (GA) obtained by oxidative cleavage of cyclopentene (CPE) with H_2O_2 catalyzed by heteropoly acid in nonaqueous medium by Furukawa et al. [11], our group has made great improvements to this interesting one-step route for the synthesis of GA from the selective oxidation of CPE [12,13]. As we know, GA is commonly used in fields of sterilization and disinfection; however, the homogeneous catalytic system restricts its further application in industry for the difficult separation and reuse of the homogeneous tungstic acid catalyst. One of the most promising ways to accomplish this aim is to design the W-containing heterogeneous catalysts. Several heterogeneous silica-supported WO_3 (i.e., WO_3/SiO_2, W-MCM-41, and W-SBA-15) and WO_3/TiO_2–SiO_2 catalysts have been designed that show good performance to the target reaction [14–18]. However, there are still many problems in the

* Corresponding authors. Fax: +86-21-65642978.
E-mail addresses: wldai@fudan.edu.cn (W.-L. Dai), knfan@fudan.edu.cn (K. Fan).

0021-9517/$ – see front matter © 2005 Elsevier Inc. All rights reserved.
doi:10.1016/j.jcat.2005.06.035

practical application of these catalysts as reported, including the complexity of the preparation procedures, the need for expensive raw materials, and the difficulties of large-scale production. Thus, efforts aimed at improving the catalyst preparation process are ongoing. Our previous work has shown that titania may be a good choice for a support of novel WO_3-based catalyst for the target reaction [18].

Titania, a widely used catalyst support [19], is known to enhance the activity in many cases due to the strong interaction between the active phase and the support [20]. Titania has three crystalline phases: rutile, anatase, and brookite. Rutile is the thermodynamically stable state, whereas the other two phases are metastable [21]. Because the crystalline state and structure of the support strongly affect the catalytic activity and selectivity, the design and selection of novel, highly active catalysts places many requirements on the supports used. Recently, much attention has been given to the synthesis of nano-structured inorganic materials with hierarchical morphologies in the fields of catalysis, separation technology, microelectronic devices, and biomaterials engineering [22–28]. In particular, the design and fabrication of spherical materials with hollow interiors has attracted considerable attention recently because of their potential applications as low-density capsules for controlled release of drugs, dyes, and inks; development of artificial cells, protection of proteins, enzymes, and DNA; and especially as supports of catalysts [29–33]. A variety of hollow particles composed of metals, ceramics, and inorganic hetero-composites of various diameters and wall thicknesses have been fabricated. So far, most of the systems reported for the formation of hollow spherical materials have been based on template-assisted processes involving the replication of organized reaction fields, such as emulsion foams [34–37], emulsion droplets, and bicontinuous microemulsions [38–41], followed by removal of the template materials by calcination or solvent etching. However, all of the aforementioned methods generally require the use of surfactants or polymers that must be removed to create the hollow interiors. Moreover, these materials are usually unstable and hence are limited in their potential applications.

In a preliminary communication, we have reported a novel simple and nonsurfactant approach to synthesizing stable core-shell structured titania microspheres with hollow interiors [42]. During this process, the novel core-shell structured titania spheres are obtained after hydrothermal precipitation of titanium chloride ($TiCl_4$) with urea in ethanol/water solution containing ammonium sulfate ($(NH_4)_2SO_4$). The as-synthesized microspheres show no agglomeration or collapse of its special structure even after calcination at 873 K for 6 h. In addition, the core-shell titania microspheres have a mesoporous structure with a narrow pore size distribution in the nanometer range, and are also thermally stable and have much more surface area than other titania material previously reported. These novel characteristics all make possible its further application as a good catalyst support; controlled-release capsules for drugs, dyes, cosmetics, and inks; and in artificial cells and fillers.

In the present work, tungsten oxide was immobilized in the interior of the core-shell titania microspheres to obtain the novel heterogeneous WO_3/TiO_2 catalyst, which was then systematically characterized by various analytical and spectroscopic techniques, including X-ray diffraction (XRD), N_2 sorption, scanning electron microscopy (SEM), transmission electron microscopy (TEM), laser Raman spectroscopy, thermogravimetric and differential thermal analysis (TG-DTA), X-ray photoelectron spectroscopy (XPS), and NH_3 temperature-programmed desorption (TPD), and was further investigated in the selective oxidation of CPE to GA with aqueous H_2O_2 under mild conditions.

2. Experimental

2.1. Catalyst preparation

2.1.1. Preparation of the core-shell titania microspheres

Certain amounts of ammonium sulfate and urea were dissolved in a dilute aqueous solution of $TiCl_4$ under ice–water bath and then combined with equal amounts of ethanol to get a mixture. The molar composition of $TiCl_4$:H_2O:EtOH:$(NH_4)_2SO_4$:$CO(NH_2)_2$ was 1:86:24:1:46. After stirring for 2–4 h, a transparent solution was obtained. The mixture was then transferred into an 200 ml autoclave, where it was heated and maintained at 368 K for 5 h. Then the autoclave was cooled to ambient temperature. The resultant slurry was filtered, washed twice with distilled water and then three times with absolute ethanol, then vacuum-dried at 353 K. Calcination of the dried titania sample was done in a muffle oven at 373–973 K in air for 3 h.

2.1.2. Preparation of the novel core-shell structured WO_3/TiO_2 catalyst

The catalyst was prepared by a conventional incipient wetness impregnation method. The required amount of ammonium tungstate was dissolved in a solution of ammonia. The as-synthesized core-shell titania microspheres was added into the stirred solution at 353 K, and the water was completely evaporated. The novel WO_3/TiO_2 catalyst was obtained after the solid material was calcined at 873 K for 3 h under air atmosphere.

2.2. Catalyst characterization

The XRD patterns were recorded on a Bruker D8 advance spectrometer with Cu-K_α radiation, operated at 40 mA and 40 kV. The laser Raman experiments were performed with a Jobin Yvon Dilor Labram I Raman spectrometer equipped with a holographic notch filter, CCD detector, and He–Ne laser radiating at 632.8 nm. The specific surface areas, pore volumes, and mean pore diameters of the samples were measured and calculated according to the BET method using a

Micromeritics Tristar ASAP 3000 BET apparatus with liquid nitrogen at 77 K. The SEM micrographs were obtained using a Philips XL 30 microscope. The samples were deposited on a sample holder with a piece of adhesive carbon tape and were then sputtered with a thin film of gold. TEM micrographs were obtained on a Joel JEM 2010 transmission electron microscope. The samples were supported on carbon-coated copper grids for the experiment. TG/DTA was performed using the Perkin Elmer TGA7/DTA7 thermal analysis system under air atmosphere (50 ml min^{-1}) with a heating rate of 10 K min^{-1}. The XPS spectra were recorded on a Perkin Elmer PHI 5000C ESCA system equipped with a dual X-ray source, of which the Al-K_α (1486.6 eV) anode and a hemispherical energy analyzer were used. The background pressure during data acquisition was maintained at $<10^{-6}$ Pa. Measurements were performed at a pass energy of 93.90 eV. All binding energies were calibrated using contaminant carbon (C_{1s} = 284.6 eV) as a reference. The NH_3 TPD experiments were conducted on a home-built apparatus. Before TPD, each sample was pretreated with high-purity (99.999%) helium flow (30 ml min^{-1}) at 773 K for 2 h, then saturated with high-purity anhydrous ammonia from a 10% NH_3 and balanced He mixture (30 ml min^{-1}) at 393 K for 1 h and subsequently flushed at the same temperature for 2 h to remove physisorbed ammonium. TPD analysis was carried out at 393–873 K at a heating rate of 10 K min^{-1}. The amount of NH_3 desorbed was calculated using CDMC GC workstation software (Shanghai Institute of Calculation Technology). The tungsten content of the WO_3/TiO_2 samples was determined by the inductively coupled argon plasma (ICP) method (IRIS Intrepid; Thermo Elemental) after the sample was solubized in HF–HCl solution.

2.3. Activity test

The activity test was performed at 308 K for 24–40 h with magnetic stirring in a closed 100 ml regular glass reactor using 50 wt% aqueous H_2O_2 as the oxygen donor and *t*-BuOH as the solvent. The molar ratio of CPE, H_2O_2, and WO_3 is 52.8:106:1, and the volume ratio of CPE and *t*-BuOH is 1:10 (mass ratio of 1:10.2). In a typical experiment, 2 ml of CPE (22.7 mmol), 20 ml of *t*-BuOH (213 mmol), and 0.6 g of the WO_3/TiO_2 (20 wt%, WO_3 ≈0.43 mmol) were introduced into the regular glass reactor at 308 K with vigorous stirring. The reaction was started by adding 2.8 ml of 50 wt% aqueous H_2O_2 (45.4 mmol) into the mixture and was maintained for 24–40 h to obtain a high conversion of CPE. The quantitative analysis of the reaction products was done by gas chromatography (GC), and the determination of different products in the reaction mixture was performed by GC-mass spectroscopy (GC-MS). Details of the method have been given elsewhere [14].

3. Results

3.1. Characterizations of the core-shell structured titania microsphere and novel WO_3/TiO_2 catalyst

The morphology of the core-shell titania microspheres and the WO_3/TiO_2 catalysts (20 wt%) was evaluated with SEM and TEM, as shown in Fig. 1. It is noteworthy that the titania microspheres produced after calcination at 773 K remained intact and maintained the three-dimensional spherical nature of particles with an average diameter of ca. 3 μm (Fig. 1a). The core-shell nature with hollow interior of the titania spheres was verified by SEM examination of deliberately broken spheres (the insert in Fig. 1a). The TEM image (Fig. 1b) shows a reduced electron density of the microspheres in the middle region of the titania spheres, suggesting that core-shell structured spheres with hollow interiors could be obtained. A wall thickness of approximately 60–80 nm is estimated by TEM (from the dark ring around the perimeter of the hollow spheres) for the titania microspheres. High-resolution TEM (the insert in Fig. 1b) shows that the shell of the core-shell titania spheres are composed of connected crystalline titania nanoparticles approximately 8–10 nm in diameter with a lattice spacing consistent with the anatase phase (0.352 nm), findings that are in good agreement with those obtained from XRD, as illustrated later.

Once tungsten oxides were supported on the core-shell titania spheres, the characteristic structure of the microspheres were maintained perfectly, except that the surface of the spheres became a little coarser, indicating excessive dispersion of WO_3 on the shell surface of the titania spheres (Fig. 1c). The TEM image (Fig. 1d) reveals that the interspaces between the core and the shell layer of titania spheres were filled up uniformly by WO_3 particles for the 20 wt% WO_3/TiO_2 catalyst (confirmed by the EDX method in TEM), which could possibly prevent the leaching of tungsten species from the WO_3/TiO_2 catalysts due to the presence of the titania shell surrounding the WO_3 layer. In addition, detailed electron microscope experiments show that the low weight content of WO_3 is first dispersed on the surface of the core and the shell layer of TiO_2, allowing WO_3 to accumulate on the interlayer of the spheroids. Once the interlayer is filled up (∼20 wt% WO_3), excess WO_3 will disperse on the outermost layer of the microspheres. For a 40 wt% WO_3/TiO_2 sample, aggregation of crystalline WO_3 is observed outside the TiO_2 microspheres, indicating that an excessive amount of WO_3 cannot lead to core-shell structured WO_3/TiO_2 material. In other words, there is a critical limit (ca. 30–40 wt%) for the WO_3 content in the as-prepared core-shell structured WO_3/TiO_2.

Nonetheless, the present preparation method can lead to the formation of well-defined mesoporous phases in the core-shell structured titania microspheres. The surface area of the samples is measured using the BET method by N_2 adsorption and desorption at 77 K. Fig. 2 shows the nitrogen

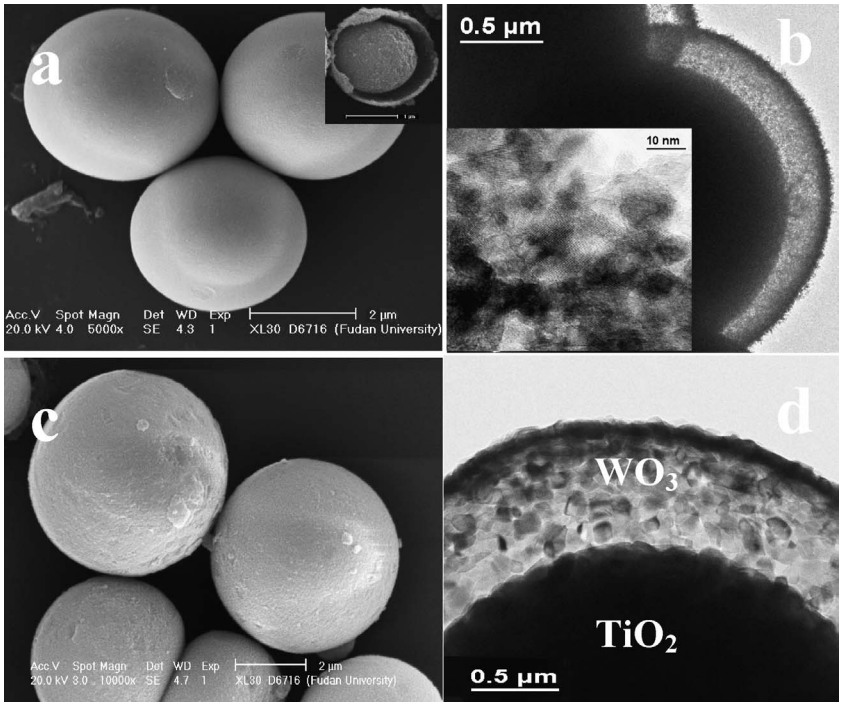

Fig. 1. SEM and TEM images of the mesoporous titania microspheres (a and b) and the 20 wt% WO_3/TiO_2 catalyst (c and d).

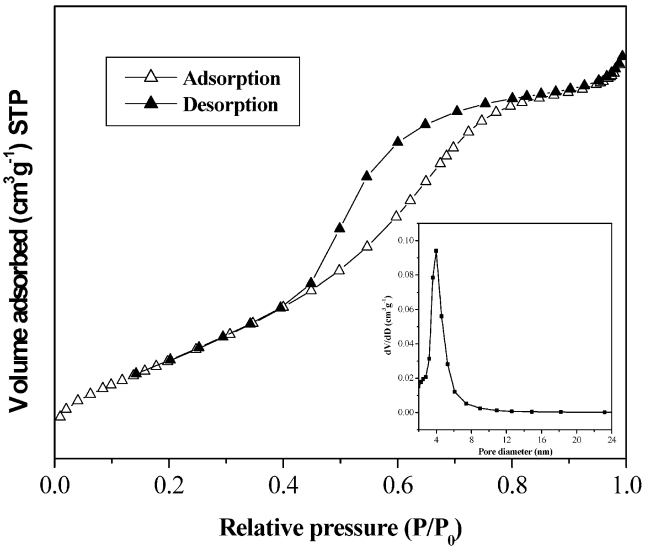

Fig. 2. Nitrogen adsorption–desorption isotherms and the corresponding pore size distribution (inset) for the calcined titania microspheres.

adsorption–desorption isotherm of the as-synthesized TiO_2 microspheres, which indicates a type IV-like isotherm with an inflection of nitrogen-adsorbed volume at $P/P_0 = 0.45$ (type H_2 hysteresis loop), indicating the presence of well-developed mesoporosity in the microspheric samples. Moreover, the insert in Fig. 2 shows the pore-size distribution plots calculated using the BJH (Barrett–Joyner–Halenda) equation from the adsorption branch of the isotherm. The pore size distribution measurement indicates that the spherical titania sample has pronounced mesoporosity of a narrow pore-size distribution with an average pore diameter

Table 1
The textural properties of the mesoporous core-shell structured titania spherical samples under different calcination temperatures

Calcination temperature (K)	BET surface area ($m^2\ g^{-1}$)	Pore volume ($cm^3\ g^{-1}$)	Pore diameter (nm)
As-synthesized	266	0.27	3.0
373	236	0.24	3.2
573	179	0.22	3.5
773	140	0.19	4.0
973	58	0.10	5.8

ca. 4.0 nm. Table 1 gives the BET surface area, specific pore volume, and pore diameter at different calcination temperatures; these values indicate a significant influence of calcination temperature on the textural properties of the titania spherical samples. As can be seen from Table 1, the BET surface area and specific pore volume obviously decreased with increasing calcination temperature whereas the pore diameter increased, indicating that the crystalline particles might become larger during the calcination process. Table 2 summarizes the physicochemical parameters of the series of WO_3/TiO_2 catalysts. The specific pore volume and pore diameter changed slightly with increasing tungsten oxide content, whereas the BET surface area decreased significantly, suggesting an obvious influence of the amount of the WO_3 on the specific surface area of TiO_2 microspheres. The tungsten contents in various WO_3/TiO_2 catalysts analyzed by ICP-AES are consistent with the values in the synthesis gel given in Table 2, suggesting that tungsten can be easily fixed on the interior of titania spheres by the conventional incipient wetness impregnation method.

Table 2
Textural parameters of titania spheroid with different WO_3 loadings

Samples	Ti/W[a] (mol)	Ti/W[b] (mol)	Surface area (m^2/g)	Pore volume (cm^3/g)	Pore diameter (nm)
5%WO_3/TiO_2	58.0	60.2	158	0.23	5.6
10%WO_3/TiO_2	29.0	30.1	124	0.23	5.8
20%WO_3/TiO_2	14.5	14.8	95	0.21	5.8
30%WO_3/TiO_2	9.7	10.2	78	0.20	5.9
40%WO_3/TiO_2	7.2	7.4	62	0.18	6.1

[a] Stoichiometric ratio in gel.
[b] Measured by ICP.

The crystalline characters of the titania spheres calcined at different temperatures were investigated by in situ XRD under air atmosphere, as shown in Fig. 3a. It is known that the as-prepared samples exhibit broad diffraction patterns characteristic of the crystal phase of anatase with a low crystallinity at ambient temperature. On increasing of calcination temperature, a sharpening of the diffraction peaks corresponding to the spheric anatase sample is observed, reflecting a slightly crystallite growth of the titania spheres. Furthermore, there are no new diffraction bands corresponding to the rutile phase being observed, suggesting that the anatase phase of titania spheres are very stable in the sample even after calcined at 973 K. Structural analysis of the WO_3/TiO_2 material with different WO_3 contents calcined at 873 K (Fig. 3b) suggests that the anatase phase of the titania spheres does not change after the impregnation of tungstate precursor whatever the difference in WO_3 content. However, the peak intensities of the corresponding reflections decrease progressively with increasing WO_3 content. With low WO_3 content, the highly dispersed tungsten oxide species cannot be detected as the crystalline phase of WO_3 by XRD; only when the loading amount equals to or exceeds 40 wt% can the residual crystalline phase of the tungsten oxide be detected, implying that the core-shell structured titania spheres can have a WO_3 loading content up to 30 wt%, but less than 40 wt%. The XRD findings are in good agreement with those from TEM and SEM.

The TG profile of the titania spheres shows a total weight loss of 20%, corresponding to the removal of adsorbed water (at <373 K; Fig. 4a), which is supported by the corresponding endothermic and exothermic transitions in the DTA profile. Moreover, there are no other endothermic or exothermic peaks in the DTA profile for titania spheres up to 1173 K. This indicates that no phase transitions occur in the titania spheres composed of much highly stable anatase crystalline phase during the calcinations process under elevated tem-

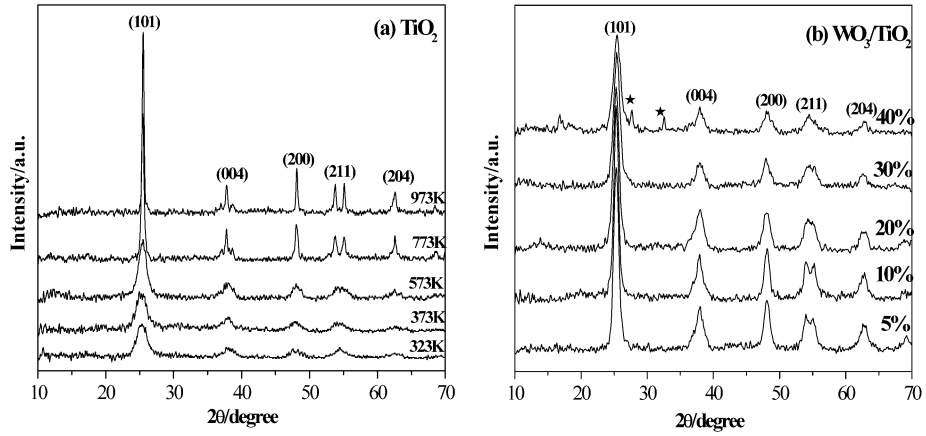

Fig. 3. (a) In situ powder XRD patterns of as-prepared mesoporous titania spheres recorded as a function of annealing temperature in air flow; (b) XRD patterns of titania spheroid samples after loading with various amounts of WO_3. ★, crystalline phase of WO_3.

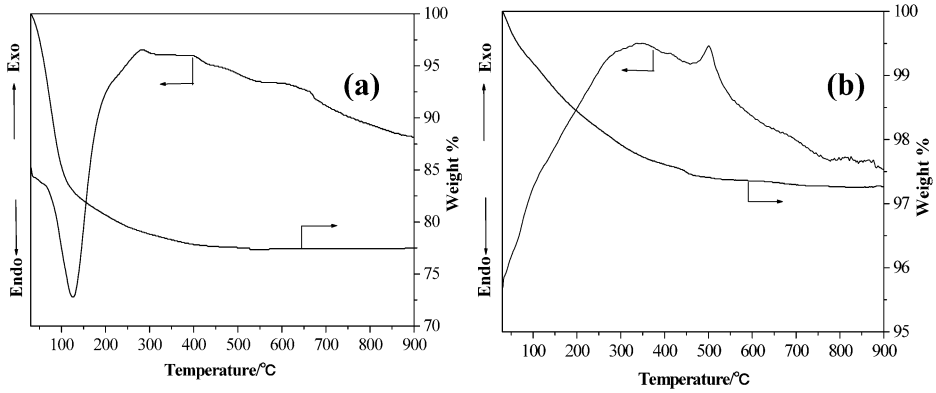

Fig. 4. TG-DTA curves of (a) titania spheroid, and (b)WO_3/TiO_2 catalyst (20 wt%).

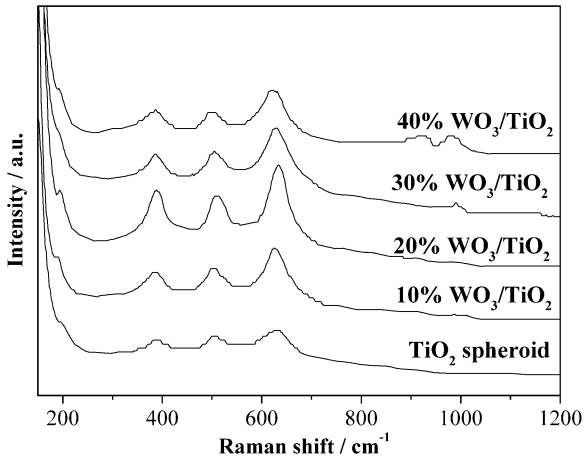

Fig. 5. Raman spectra of titania spheroid with different WO_3 loadings.

perature. Similar results can be observed with in situ XRD. However, the DTA curve of the WO_3/TiO_2 catalyst (20 wt%) shows an exothermic peak at ca. 753 K (Fig. 4b). Compared with the DTA curve of blank titania spheres, this exothermic peak may be ascribed to the interaction between tungsten oxide species and titania supports, because no such a peak appeared at this temperature for the pure titania spheres. Therefore, it can be concluded that the special core-shell structured titania spheres not only improve the dispersion of WO_3, but also strengthen the interaction of the tungsten oxide species with titania support [20].

The Raman spectra recorded at room temperature, shown in Fig. 5, provide additional information about the WO_3 structure dispersed in the interlayer of core-shell structured titania spheres with different WO_3 contents. The Raman bands of those WO_3/TiO_2 catalysts (WO_3 <30 wt%) are very similar to those of the pure titania spheres; however, new Raman bands appear, except those characteristic of anatase, for the sample with much higher WO_3 content. The titania sphere exhibits typical anatase Raman bands at 144, 199, 399, 520, and 643 cm^{-1} [43], which makes the detection of Raman bands of tungsten oxide difficult, because typical Raman bands of WO_3 are similar to those of anatase in this region (e.g., 267, 327, 714, and 804 cm^{-1}) and are overlapped by strong, broad bands of anatase. However, two new bands at 935 and 984 cm^{-1} are observed for the WO_3/TiO_2 catalyst with much higher loading of tungsten oxide (30 and 40 wt%). As we know, identification of the tungsten oxide species on the support requires W=O stretching frequencies of octahedral tungsten oxide units of 740–980 cm^{-1} and the W=O stretching frequencies of the tungsten–oxygen tetrahedral units of 913–1060 cm^{-1}. The stronger Raman signal from tetrahedral unit structures of surface tungsten oxides is due to their higher W–O bond order compared with that of the octahedral structures. Thus, the Raman spectra of samples with both structures are dominated by bands assigned to tungsten oxide tetrahedra [44]. In the present work, weak bands due to tetrahedral tungsten oxide are seen for only the 30 and 40 wt% WO_3 samples, clearly indicating that tungsten oxide species are uniformly dispersed on/in the titania spheres when WO_3 loadings are not >20 wt%.

XPS investigation of binding energies and intensities of the surface elements provides information on the chemical states and relative quantities of the outermost surface compounds. Fig. 6a shows the Ti_{2p} XPS spectra of the WO_3/TiO_2 catalysts after calcination at 873 K as a function of tungsten oxide content. It can be observed that for the pure titania spheres, the XPS signal of $Ti_{2p_{3/2}}$ can be fitted with two components (Fig. 6b), one located at 458.9 eV, attributed to Ti(IV) species, and the other located at 458.0 eV, assigned to Ti(III) species [45,46]. This indicates that there are two types of titanium oxide species on the surface of the core-shell structured titania spheres, with relative amounts of the Ti(IV) and Ti(III) species about 78.7 and 21.3%, respectively. However, all of the WO_3/TiO_2 catalysts with different WO_3 loadings do not show Ti(III) species at $Ti_{2p_{3/2}}$ binding energy values around 458.0 eV, indicating that the Ti(III) species present in the surface of the novel core-shell structured TiO_2 microspheres disappear when WO_3 is incorporated. This result also confirms that lattice oxygen transfers from WO_3 to TiO_2 and interactions between WO_3 and

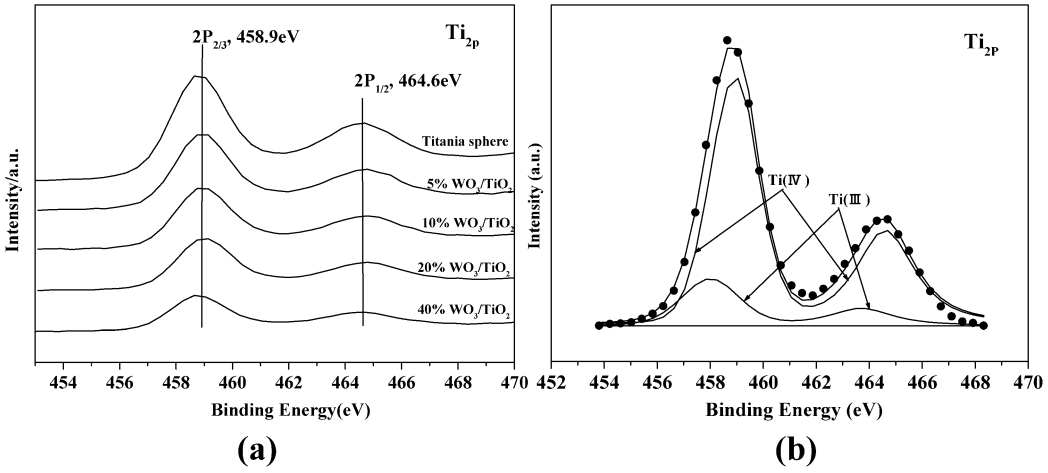

Fig. 6. (a) Ti_{2p} XPS spectra of TiO_2 spheroid with different WO_3 loading; (b) peak-fitting XPS spectrum of Ti_{2p} of the as-synthesized titania sphere.

Table 3
Proportion of the surface species of titania sphere and various WO_3/TiO_2 samples

Sample	W[a] (mol%)	Ti[b] (mol%)	O[c] (mol%)	W^{5+}/W[d]	Ti^{3+}/Ti^{4+} [e]	WO_3/TiO_2 (wt%)	O-defic. (mol%)**
Titania sphere	0	34.0	66.0	0	0.2	0	2.9
5 wt% WO_3/TiO_2	2.0	33.1	64.9	0.48	0	17.5	10.1
5 wt% WO_3/TiO_2 *	1.8	33.6	64.6	0.50	0	15.5	11.0
10 wt% WO_3/TiO_2	3.2	30.9	65.9	0.40	0	30.0	7.7
10 wt% WO_3/TiO_2 *	3.3	30.7	66.0	0.42	0	31.2	7.4
20 wt% WO_3/TiO_2	5.1	28.4	66.5	0.34	0	52.1	7.8
20 wt% WO_3/TiO_2 *	5.4	28.3	66.3	0.36	0	55.3	8.9
40 wt% WO_3/TiO_2	7.3	25.6	67.0	0.38	0	82.7	8.7
40 wt% WO_3/TiO_2 *	7.6	25.3	67.1	0.39	0	87.1	8.6

[a,b,c,e] Calculated according to the peak areas of W_{4d}, Ti_{2p} and O_{1s}, respectively.

[d] Calculated according to the curve-fitting results of the W_{4f} XP spectra of catalysts: * after Ar^+ etching for 15 min; ** calculated from the determined as compared with the theoretical oxygen content by XPS according to the equation: O-defic.% = (W% × 3 + Ti% × 2 − O%)/(W% × 3 + Ti% × 2).

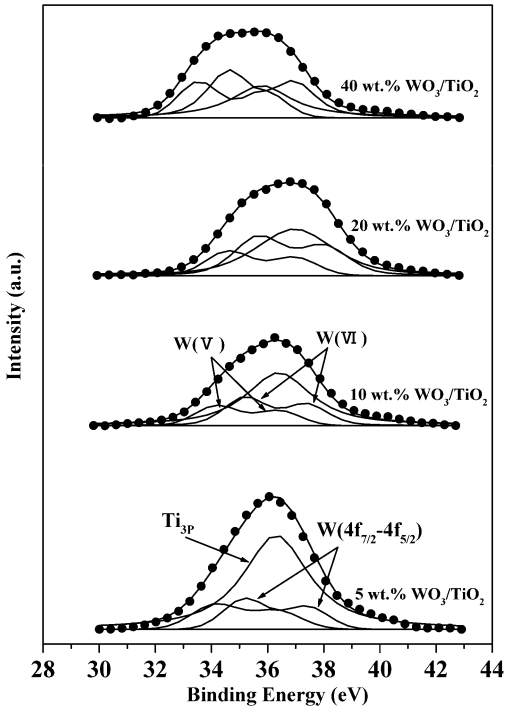

Fig. 7. XPS spectra of the W_{4f} region for different WO_3/TiO_2 catalysts.

TiO_2 exist when WO_3 is doped in the interlayer of the TiO_2 microspheres. In addition, as seen from Fig. 6, the XPS signal intensity of the Ti_{2p} obviously decreases after tungsten species are incorporated. Peak-fitting results of W_{4f} XPS spectra corresponding to different samples are summarized in Fig. 7. Detailed quantitative results from the peak-fitting results of W_{4f} and O_{1s}, as well as Ti_{2p}, are given in Table 3.

In the present work, two energy levels of tungsten were measured in the W_{4d} and the W_{4f} region. The W_{4d} peak is broad and cannot be used to determine the oxidation state of tungsten, but it is useful to quantify the amount of tungsten on the support. The quantitative surface composition results for the WO_3/TiO_2 catalysts before and after 15 min of Ar^+ etching are also included to explore the differences in composition between the top surface and the subsurface of the novel core-shell structured WO_3/TiO_2 catalyst. However, analysis of the W_{4f} region is complicated by interference from the Ti_{3p} level of the TiO_2 support, especially when tungsten is highly oxidized, that is, when it has a high binding energy. By the curve-fitting procedure based on the theory of Doniach and Sunjic [47,48], it is possible to distinguish between the two signals and to determine the valence of tungsten from the position of the W_{4f} level. The measured spectra appear similar for all samples and show identical positions for the W_{4f} peaks, except for the minor charging effect observed and corrected for according to the contaminant carbon (C_{1s} = 284.6 eV). Both W(VI) and W(V) species at $W_{4f_{7/2}}$ (of 35.2 and 34.2 eV [49]) for the W_{4f} spin-orbit components have been detected. With increasing tungsten oxide loading, the intensity of the W_{4f} XPS peaks also increases before and after Ar^+ etching, as illustrated by the changes in relative peak areas for W_{4f} and Ti_{3p} shown in Fig. 7. Table 3 also gives the quantitative results of the weight ratio of WO_3 on TiO_2 by XPS according to the relative peak intensity of W_{4f} and Ti_{2p} after correction with atomic sensitivity factors; these can be easily compared with the as-added values in the table's first column. It is interesting to note that the surface WO_3 content is much higher than the mean values as directly mixed. For the 5% WO_3/TiO_2 catalyst, the actual surface weight ratio of WO_3 on TiO_2 is 17.5%, 3.5 times higher than the mean value of WO_3 as added in the TiO_2 support. However, it is clear that the enhancement of this ratio with the weight percentage of tungsten is not linear, suggesting that deposition of the tungstate surface species is not uniform with increasing tungsten loading and that the deviation from linearity is obtained between the catalysts at WO_3 loading >20%. Fig. 8 clearly shows the relationship between the surface molar ratio of W/Ti and that of the mean value as added, which is in good agreement with that of the results listed in Table 3. These XPS results show that surface enrichment of WO_3 is obviously observed for all of the WO_3/TiO_2 catalysts, suggesting that WO_3 is dispersed on the surface of the core-shell structured TiO_2. Thus the XPS results are in line with the TEM results shown in Fig. 1.

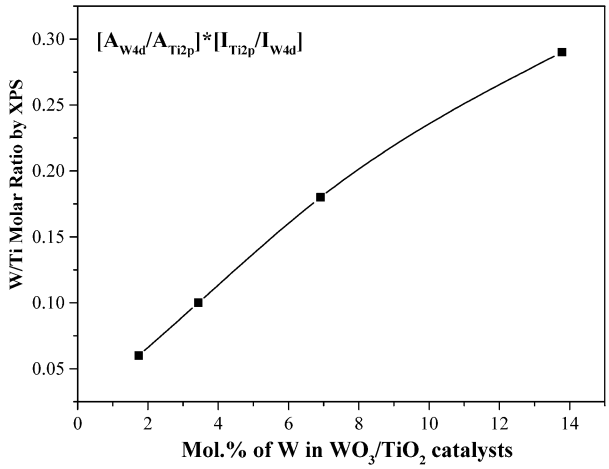

Fig. 8. W/Ti surface ratios as a function of tungsten content (wt%) on various WO_3/TiO_2 catalysts.

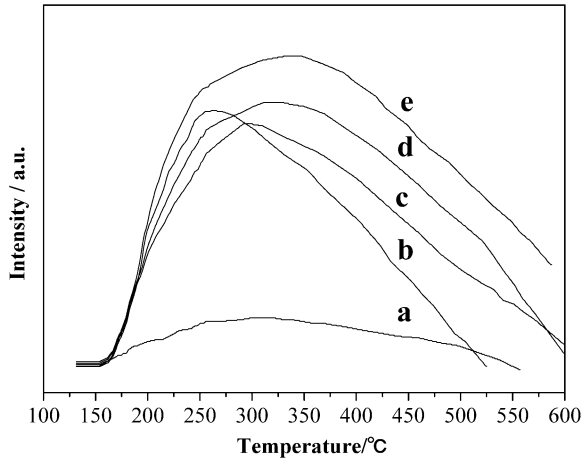

Fig. 9. NH_3-TPD profiles of various WO_3/TiO_2 catalysts. (a) TiO_2 spheroid; (b) 20% WO_3/TiO_2(A); (c) 10%; (d) 20%; (e) 30% WO_3/TiO_2 spheroid.

From Table 3 and Fig. 7, another interesting phenomenon can be observed. A great amount of W^{5+} exists regardless of the Ar^+ etching, which accords well with the existence of oxygen deficiency as determined by quantitative XPS given in the last column of Table 3. With the increase of the tungsten loading, the ratio of W^{5+} first decreased from ca. 50 to ca. 35% when the WO_3 loading increased from 5 to 20%, then increased slightly to ca. 40% at 40 wt% of tungsten loading, which is somewhat in agreement with the trend for changes in oxygen deficiency. In addition, the oxygen deficiency content increases abruptly from 2.9 to 10.1% after 5% WO_3 is loaded, suggesting that much more oxygen deficiency is produced after WO_3 is introduced into the interior of the core-shell structured TiO_2 spheroids. However, although there are some deviations in the data of Table 3 for the samples after Ar^+ etching compared with those before Ar^+ etching, most are similar, considering the errors for quantitative XPS, indicating that the surface composition of the core-shell structured WO_3/TiO_2 catalyst is uniform in the detection limit of XPS considering the Ar^+ etching experiments in the present work (<20 nm). Based on the changes in surface tungsten content with increasing tungsten loading, it can be assumed that tungsten species are dispersed in the interspaces between the core and the shell of the titania spheres with WO_3 loadings equal to 20 wt%, and that further increases in WO_3 loading will lead to the agglomeration of tungsten oxide species onto the outside surface of the titania spheres. In addition, the existence of oxygen deficiency and the interaction of tungsten oxide with titania provide abundant oxygen defect lattices for catalytic oxidation [46,50,51], which is considered to play a key role in the selective oxidation of CPE to GA.

TPD of probe molecules like ammonia and pyridine is a popular method for determining the acidity of solid catalysts as well as acid strength [52]. In the present investigation, the acidity measurements were carried out with the ammonia TPD method. It is well known that tungsten trioxide has Lewis acid sites [53]. If porous materials contain deposited tungsten oxide species, then acid centers will be generated and ammonia adsorption–desorption effects should be observed. The NH_3 TPD profiles of the WO_3/TiO_2 samples are presented in Fig. 9. The acidity values and TPD peak positions are given in Table 4. There is only one asymmetric broad peak on the TPD profiles of all the samples, and the peak temperatures are ranged between 473 and 673 K, indicating that most of the acid sites of the samples are of medium-strong strength. As expected, pure titania shows low ammonia desorption because of the lack of acid centers. In contrast, there is a broad peak of ammonia desorption as the tungsten oxide species are dispersed on/into the titania spheres; moreover, the acidity value increases and the desorption temperature shifts to a higher position, indicating acidity increases with increasing tungsten content in the WO_3/TiO_2 samples. However, the conversion value during the selective oxidation of CPE to GA is found to decrease at 30 wt% WO_3, indicating that excessive acidity is not beneficial to selective oxidation as mentioned. Table 4 also gives the acidity value and temperature position of 20 wt% WO_3 catalyst with the commercial anatase titania as the support [denoted as WO_3/TiO_2(A)]. Compared with the 20 wt% WO_3/TiO_2(A) sample, the 20 wt% WO_3/TiO_2 spheric sample has more acidic amount and stronger acidic strength, pointing to a chemical reaction or interaction between the tungsten oxide species and titania spheres that may be helpful to the selective oxidation of CPE.

Table 4
Summary of NH_3-TPD data upon various WO_3/TiO_2 catalysts

Samples	T_d (°C)	Acidic amounts ($mmol_{NH_3}/g_{cat}$)
TiO_2 spheroid	290	0.296
10%WO_3/TiO_2 spheroid	295	0.752
20%WO_3/TiO_2 spheroid	316	0.896
30%WO_3/TiO_2 spheroid	328	1.154
20%WO_3/TiO_2(A)	261	0.623

Table 5
Performance of catalytic oxidation of CPE over various 20% WO_3/TiO_2[a]

Substrates	Time on stream (h)	Conversion of H_2O_2 (%)	Conversion of CPE (%)	Selectivity (%)			
				CPO	GA	CPLE	CPDL
TiO_2(R)	40	98	43.6	31.0	40.1	15.1	13.8
TiO_2(A)	40	99	70.5	7.2	69.6	11.1	12.1
TiO_2 spheroid	40	99	95.0	17.8	72.9	4.2	5.2

[a] Reaction conditions: 2 ml cyclopentene, 2.8 ml 50% H_2O_2, 20 ml *t*-BuOH, 0.6 g catalyst, the molar ratio of CPE:H_2O_2:WO_3 = 52.8:106:1, the volume ratio of CPE:*t*-BuOH = 1:10, T = 308 K. CPE, cyclopentene; CPO, cyclopentene-epoxide; GA, glutaraldehyde; CPDL, cyclopentan-1,2-diol; CPLE, 2-*t*-butyloxy-1-cyclopentanol.

Table 6
Influence of WO_3 loading in the WO_3/TiO_2 spheroid catalysts system[a]

Content of WO_3 (%)	Time on stream (h)	Conversion of CPE (%)	TOF[b] (h^{-1})	Selectivity (%)			
				CPO	GA	CPLE	CPDL
10	35	74	1.12	21.2	75.8	3.01	0.0
20	40	95	1.25	17.8	72.9	4.2	5.2
30	40	96	1.26	18.3	62.2	9.0	10.5
40	36	90	1.32	20.9	64.4	11.1	3.6

[a] Same as in Table 5.
[b] Calculated according to the equation as: TOF = moles of CPE per moles of WO_3 per hour.

3.2. Catalytic tests in the selective oxidation of CPE to GA

The catalytic performance of selective oxidation of CPE to GA over the 20 wt% WO_3/TiO_2 catalysts with different titania as supports is delineated in Table 5. As shown in the table, the catalytic performance of the catalysts with anatase-phase titania [TiO_2(A)] as the support is better than that of the catalysts with rutile-phase titania [TiO_2(R)] for the selective oxidation of CPE to GA, not only in terms of the conversion of CPE (70.5 to 43.6%), but also in terms of the selectivity toward GA (69.6 to 40.1%); however, the specific mechanism responsible for this finding is not yet clear. According to results of previous work [12,14], the mechanism from CPE to GA is through an epoxidation route that first produces cyclopentene-epoxide (CPO) and then yields GA through the oxidation of CPO in the presence of hydrogen peroxide. As Table 5 also shows, GA is inclined to form on the former catalyst, whereas much more cyclopentene oxide is formed on the latter catalyst, suggesting that epoxidation reaction occurs easily over WO_3-based catalyst supported on rutile-phase titania, whereas deep oxidation is apt to occur over catalysts supported on anatase TiO_2. Furthermore, the WO_3/TiO_2 catalyst using core-shell structured titania sphere as the substrate has a much higher GA yield (69.3%) than the commercial anatase phase of titania (49.1%) under same reaction conditions. All of the results indicate that both the crystalline phase and the structure of the titania support for the WO_3/TiO_2 catalyst strongly influence catalytic activity and selectivity in the selective oxidation of CPE to GA with aqueous H_2O_2 as the oxygen donor.

Table 6 reports the catalytic performance over various W-containing catalysts with different tungsten trioxide content. For the purpose of comparison, the catalysts used in these experiments contain the same amount of tungsten. As shown in Table 6, GA yield is strongly dependent on the tungsten content of the WO_3/TiO_2 catalysts, and the optimum catalyst in the present reaction is the one with 20 wt% of WO_3. When WO_3 content is <20%, a low GA yield is obtained. Conversely, if the WO_3 content is >20%, inevitable agglomeration of WO_3 and the much stronger acidity of the WO_3/TiO_2 catalysts lead not only to lower CPE conversion, but also to lower GA yield. The 20 wt% WO_3/TiO_2 catalyst shows 95% CPE conversion and 69.3% GA yield, a little higher than that reported previously in this reaction system using a WO_3/TiO_2–SiO_2 catalyst [18] synthesized through a complex procedure using the sol–gel method. It should also be noted that the catalysts reported by our group earlier all have one big drawback—it is very difficult to separate the solid catalyst from the reaction mixture after the reaction is completed, because of the low density and the ultrafine particle size of the catalysts. Therefore, applying these WO_3-based catalysts in industry is hindered by the difficulties entailed in their separation and large-scale production. However, the present novel core-shell structured WO_3/TiO_2 catalyst has a spheric appearance with 2–3 μm diameter, is very easily separated from the reaction mixture by simple filtration, and needs no costly raw materials for its preparation. Moreover, this type of catalyst with a special core-shell structure has a much greater mechanic intensity than other similar materials and can be easily produced on a large scale. As discussed later, this catalyst is very thermally stable, and the active WO_3 species will not leach into the reaction mixture after numerous reaction cycles. Thus this novel catalyst seems to be a promising candidate for further application in industry. The great difference in catalytic performance among the WO_3/TiO_2 catalysts with different tungsten content suggests that the presence of the highly dispersed tungsten species on/into the titania is necessary for the title reaction. The TOF values (also shown in Table 6) show little difference among those catalysts with different WO_3 content, indicating that the mean conversion rate of CPE over different WO_3/TiO_2 catalysts is similar during the reaction process for about 35–40 h. However, the selectivity toward GA is much higher (>10%) over 10 and 20% WO_3/TiO_2 catalysts than over 30 and 40% ones, causing the large differences in GA yield over these WO_3/TiO_2 catalysts. These findings suggest that there are intrinsic differences in the WO_3 dispersed in the TiO_2 microspheres with

Table 7
Catalytic performance of various amounts of 20%WO_3/TiO_2 spheroid[a]

Amounts (g)	Time on stream (h)	Conv. of H_2O_2 (%)	Conv. of CPE (%)	TOF[b] (h^{-1})	Selectivity (%)			
					CPO	GA	CPLE	CPDL
0.2	43	100	83	2.54	19.5	72.5	6.6	1.4
0.5	40	100	95	1.25	17.8	72.9	4.2	5.2
0.8	30	100	99	1.09	17.3	73.6	5.4	3.7

[a,b] Same as in Table 6.

Table 8
Catalytic performances of catalytic oxidation of CPE over various concentration of hydrogen peroxide[a]

Concentration of H_2O_2 (wt%)	Time on stream (h)	Conversion of H_2O_2 (%)	Conversion of CPE (%)	Selectivity (%)			
				CPO	GA	CPLE	CPDL
30	40	99	83	18.5	71.5	5.6	4.4
50	40	100	95	17.8	72.9	4.2	5.2
70	24	100	98	18.0	74.2	3.5	4.3

[a] 0.6 g 20 wt% WO_3/TiO_2, others are same as in Table 5.

different WO_3 content. Considering the reaction rate as well as the selectivity to GA, the 20% WO_3/TiO_2 catalyst is the optimal one for the selective oxidation of CPE to GA.

The reaction results as a function of the amounts of 20 wt% WO_3/TiO_2 catalyst used were also investigated, and are listed in Table 7. It was found that the conversion of CPE increases with increasing amounts of the catalyst used in the oxidative reaction in a fixed reaction period, suggesting that the reaction rate is accelerated with the increasing amounts of catalyst. In addition, the selectivity toward GA increases slightly with increasing amounts of catalyst, whereas the TOF values first decrease significantly when the catalyst amount is increased from 0.2 to 0.5 g, then decrease slightly when the catalyst amount is increased further from 0.5 to 0.8 g; this may be interpreted with the changes in mass transfer during the changes in catalyst amount. The only slight differences in GA selectivity can be easily explained based on the same nature of WO_3 active species in the 20% WO_3/TiO_2 catalyst.

The weight content of H_2O_2 in its aqueous solution used in the present study plays an important role in the selective oxidation of CPE over the 20 wt% WO_3/TiO_2 spheroid catalyst. As shown in Table 8, an increasing H_2O_2 concentration obviously leads to a corresponding increase in CPE conversion as well as GA selectivity, which can be readily ascribed to the accelerated reaction rate and the decreased water content in the reaction mixture. Similar phenomena were also observed in our previous work [12–18], and were interpreted accordingly with the parallel one-order reaction mechanism. In addition, a surprising GA yield (72.7%) was obtained when a 70% H_2O_2 was used, which was 7.7% higher than that obtained over homogeneous tungstic acid catalyst (∼65%). However, it is not safe to handle an aqueous H_2O_2 solution with a concentration >50%, especially in large-scale industrial production. Hence a 50-wt% aqueous solution of H_2O_2 is a suitable oxidant for future use in industry.

Table 9
Recycling results of novel 20%WO_3/TiO_2[a] catalyst

Cycle index	Conversion of CPE (%)	Conversion of H_2O_2 (%)	Yield of GA (%)	Selectivity of GA (%)
0	95	98	69	73
1	94	98	66	70
2	93	95	60	66
3	90	94	56	64
4	87	92	55	63
5	85	92	54	63
6	85	91	53	62
6^R	94	98	68	72

Superscript "R" denotes "after regeneration."
[a] Same as in Table 8.

To investigate the stability and duration of the core-shell structured WO_3/TiO_2 (20 wt%) spheroid catalyst, the leaching of WO_x species into the reaction mixture and the tungsten remaining in the catalyst were also determined after six reaction cycles. No detectable leaching of W species or obvious loss of tungsten in the WO_3/TiO_2 samples could be observed, indicating the presence of strong interactions between active tungsten species and the spheric titania support. Similar effects were also observed by Strukul et al. using niobium-based catalyst in the epoxidation of olefins with hydrogen peroxide as the oxidant [54]. Table 9 gives the results of the selective oxidation of CPE to GA over WO_3/TiO_2 (20 wt%) catalyst with different reaction cycles and the postregeneration material. As shown, GA yield decreases slowly and remains above 50% even after the sixth cycle. After six reaction cycles, the used WO_3/TiO_2 (20 wt%) catalyst was characterized by XRD (not shown). The results show the appearance of crystalline WO_3, possibly related to the decrease in activity. However, after calcination at 823 K in air for 2 h, all of the crystalline WO_3 peaks disappear, and the outstanding catalytic activity can be recovered, indicating that tungsten species are uniformly dispersed once again. In addition, XPS found a small amount of contaminant car-

bon on the surface of the used WO_3/TiO_2 catalyst that can be removed after calcination at 823 K in air for 2 h. Therefore, the appearance of crystalline WO_3 and the surface contaminant carbon, which must result in a decrease of the active centers, is the main reason for the decrease in GA yield during the recycling process of the novel WO_3/TiO_2 catalyst. In conclusion, the WO_3/TiO_2 (20 wt%) catalyst shows high stability and activity for the selective oxidation of CPE to GA and can be regenerated by simple calcination in air.

Another experiment was performed to test whether this novel WO_3/TiO_2 catalyst is actually heterogeneous. After carrying out the reaction over WO_3/TiO_2 catalyst for 10 h, the catalyst was removed through simple filtration and the reaction solution was stirred for another 14 h. No detectable increase of GA yield and CPE conversion were observed during the 14 h of reaction, indicating that the trace amount of leached W species has almost no detectable catalytic effect on the reaction; the leaching of tungsten species from WO_3/TiO_2 (20 wt%) was <1.0 ppm in one reaction cycle, as determined by ICP.

4. Discussion

In this work we have demonstrated a new preparation method for thermally stable core-shell structured titania microspheres with hollow interiors by using a novel hydrothermal precipitation technology. We also have investigated the catalytic application of this novel core-shell structured TiO_2 with hollow interiors as supports of active species WO_3 in the selective oxidation of CPE to GA. We believe that the hollow structures of the titania materials are associated with a two-step precipitation of the titania species from the reaction systems as shown in Scheme 1: (i) formation of a homogeneous ethanol/water solution of $TiCl_4$, urea, and ammonium sulfate [see Scheme 1a] and (ii) a subsequent hydrothermal precipitation of the foregoing reaction mixture to form TiO_2 microspheres [see Scheme 1b]. In this respect, the ammonium sulfate present can behave as an electrolyte and thus modify the zeta potential of spherical polycondensed titania species generated at the initial stage of the hydrolysis reaction [55]. The hollow interiors may therefore be created from the subsequent precipitation of the titania species onto the ammonium sulfate-stabilized spherical titania surrounded by the ammonium sulfate dissolved in $EtOH/H_2O$ solutions in the reaction systems [see Scheme 1c]. The core-shell structured titania spheres thus may be produced after calcinations at 773 K for 3 h [see Scheme 1d]. It is interesting to find that the as-prepared core-shell structured titania spheres present only the anatase phase approved by XRD even after calcination at 973 K. Moreover, BET characterization by the N_2 adsorption and desorption method shows that the titania spheres have well-defined mesophases, large specific area, and high surface permeability, making them potentially useful in further applications as catalysts or supports. In the present work, WO_4^{2-} was introduced after mixing of aqueous solution of ammonium tungstate with TiO_2 microspheres [see Scheme 1e]; highly dispersed WO_3 appeared after the excess water was removed and ammonium tungstate was decomposed to tungsten oxide at elevated temperature [see Scheme 1f].

The novel WO_3/TiO_2 catalyst was prepared by the conventional incipient wetness impregnation method using core-shell structured titania spheres as the support. This catalyst exhibits high activity and selectivity in the selective oxidation of CPE to GA with aqueous H_2O_2 as the oxidant. The simple preparation method and the high CPE conversion (95%) and relatively high GA yield (69.3%) combine to make this a promising candidate for further application in industry. TEM studies proved that the tungsten oxide species are highly dispersed in the interspaces between the core and the shell layer of the titania spheres at a WO_3 content <20 wt%. XRD patterns and laser Raman spec-

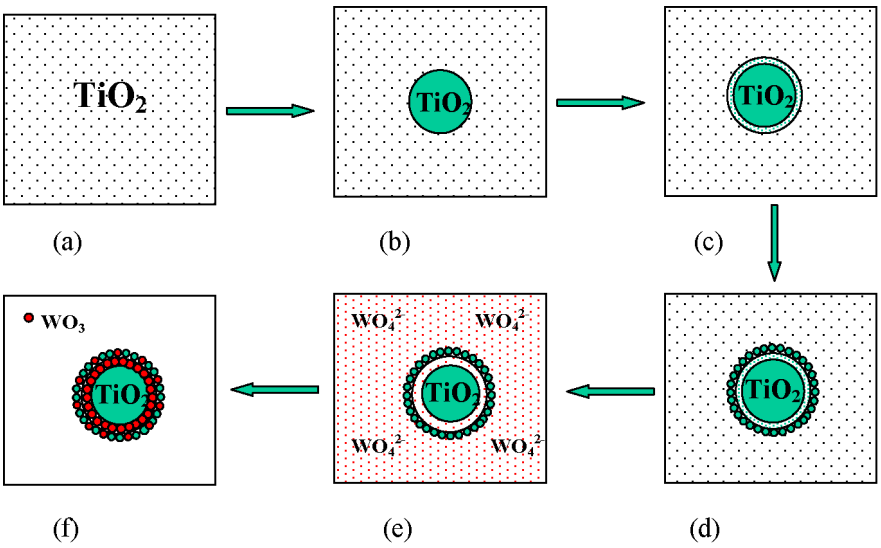

Scheme 1. The process for the formation of core-shell structured WO_3/TiO_2 catalyst.

tra also indicated the presence of highly dispersed WO_3 on the TiO_2 support with increasing WO_3 loading. With WO_3 content <20 wt%, the tungsten species are uniformly dispersed, which cannot be detected by XRD or laser Raman spectroscopy. With WO_3 content >20%, the dispersed WO_3 begins to crystallize into small WO_3 particles. These small WO_3 particles, which cannot be detected by XRD but can be detected by laser Raman spectroscopy, lead to the slightly decreased catalytic performance. With further increases in WO_3 loading up to 40 wt%, the crystalline WO_3 appears on the surface of the titania spheres, as also confirmed by Ar^+-etching XPS, which results in a significantly decreased GA yield in the selective oxidation of CPE. Even then, the incorporation of 40 wt% tungsten oxide species does not change the crystalline phase of the TiO_2 support, which still presents as an anatase-phase form, suggesting the great stability of the anatase phase in the special core-shell structured TiO_2 spheres.

XPS results show that two types of tungsten oxide with oxidation states of 6+ and 5+ are present in the novel core-shell structured WO_3/TiO_2 catalyst, whereas titanium oxide has only one oxidation state of titanium ($\sim Ti^{+4}$) in this catalyst. The low oxidation state of tungsten (W^{+5}) in the highly dispersed tungsten oxide provides abundant W^{+5}–O species to produce abundant oxygen defect lattices, which is considered helpful in increasing the activity of the WO_3/TiO_2 catalyst. TG-DTA and XPS characterizations of the WO_3/TiO_2 catalyst demonstrate that the tungsten species are highly dispersed on the titania spheres and that there are strong interactions between the tungsten species and the support, preventing leaching of the tungsten species during the selective oxidation of CPE to GA with aqueous hydrogen peroxide. In addition, the catalyst shows much high stability and can be reused as many as six times. The diminished catalytic performance results from the appearance of crystalline WO_3 and the surface contaminant, which can be removed by simple calcination.

5. Conclusions

In this work, a novel thermally stable core-shell structured WO_3/TiO_2 catalyst was synthesized by the traditional incipient wetness impregnation method using ammonium tungstate as the W source and core-shell structured titania microspheres as supports. The special hollow interiors of these microspheres were prepared using a novel hydrothermal precipitation technology. According to the results from various characterizations, WO_3 species are highly dispersed in the interspace of titania spheres to form the novel WO_3/TiO_2 catalyst, and there is strong interaction between WO_3 and the TiO_2 support. The high dispersion of the tungsten species achieved on the core-shell structured titania spheres, the strong interaction, and the medium-strong acidity of the catalyst are all considered to contribute to the superior catalytic behavior of the WO_3/TiO_2 catalyst in the selective oxidation of CPE to GA. The optimal tungsten content is 20 wt%, and the GA yield over this catalyst reaches 69.3%, suggesting its potentially promising use in industry.

Acknowledgments

This work was supported by the Major State Basic Research Development Program (grant 2003CB615807), the NSFC (projects 20407006, 20473021, and 20203003), the Natural Science Foundation of Shanghai Science & Technology Committee (02DJ14021), and the Committee of Shanghai Education (02SG04).

References

[1] Z.Y. Zhong, Y.D. Ying, B. Gates, Y.N. Xia, Adv. Mater. 12 (2000) 206.
[2] F. Somma, G. Strukul, J. Catal. 227 (2) (2004) 344.
[3] G. Strukul (Ed.), Catalytic Oxidations with Hydrogen Peroxide as Oxidant, Kluwer Academic, Dordrecht, the Netherlands, 1992.
[4] B.F. Sels, D.E. De Vos, P.A. Jacobs, Angew. Chem. Int. Ed. 44 (2) (2005) 310.
[5] R.D. Wilson, D.G. Barton, C.D. Baertsch, E. Iglesia, J. Catal. 194 (2000) 175.
[6] J. Engweiler, J. Harf, A. Baiker, J. Catal. 159 (1996) 259.
[7] Y. Ishii, K. Yamawaki, T. Ura, H. Yoshida, M. Ogana, J. Org. Chem. 53 (1988) 3587.
[8] M. Oguchi, T. Ura, Y. Ishii, M. Ogana, Chem. Lett. 857 (1989).
[9] G.M. Karagezyan, USSR SU Patent 878760 (1981).
[10] JP Patent 59108734 (1984), to Daicel Chemical Industries Ltd. Co.
[11] H. Furukawa, E. Nishikawa, T. Koyama, Patent JP 6219546 (1987).
[12] J.F. Deng, X.H. Xu, H.Y. Chen, A.R. Jiang, Tetrahedron 48 (1992) 3503.
[13] W.L. Dai, X.J. Huang, H.Y. Chen, J.F. Deng, Indian J. Chem. B 36 (1997) 583.
[14] R.H. Jin, H.X. Li, J.F. Deng, J. Catal. 203 (2001) 75.
[15] H. Chen, W.L. Dai, J.F. Deng, K.N. Fan, Catal. Lett. 81 (2002) 31.
[16] W.L. Dai, H. Chen, Y. Cao, H.X. Li, S.H. Xie, K.N. Fan, Chem. Commun. 7 (2003) 892.
[17] X.L. Yang, W.L. Dai, H. Chen, Y. Cao, H.X. Li, H.Y. He, K.N. Fan, J. Catal. 229 (2005) 259.
[18] R.H. Jin, X. Xia, W.L. Dai, J.F. Deng, H.X. Li, Catal. Lett. 62 (1999) 201.
[19] C.N. Satterfield, Heterogeneous Catalysis in Industrial Practice, second ed., McGraw–Hill, New York, 1991, p. 123.
[20] M. del Arco, A. Caballero, P. Malet, V. Rives, J. Catal. 113 (1988) 120.
[21] M. Gopal, W.J. Moberlychan, L.C. De Jonghe, J. Mater. Sci. 32 (1997) 6001.
[22] L. Radtchenko, G.B. Sukhorukov, N. Gaponik, A. Kornowski, A.L. Rogach, H. Mohwald, Adv. Mater. 13 (2001) 1684.
[23] C.T. Kresge, M.E. Leonowicz, W.J. Roth, J.C. Vartuli, J.S. Beck, Nature 359 (1992) 710.
[24] H. Yang, N. Coombs, G.A. Ozin, Nature 386 (1997) 692.
[25] D. Zhao, J. Feng, Q. Huo, N. Melosh, G.H. Fredrickson, B.F. Chmelka, G.D. Stucky, Science 279 (1998) 548.
[26] P.V. Braun, P. Osenar, S.I. Stupp, Nature 380 (1996) 325.
[27] J. Liu, Y. Shin, Z. Nie, J.H. Chang, L.Q. Wang, G.E. Fryxell, W.D. Samuels, G.J. Exarhos, J. Phys. Chem. A 104 (2000) 8328.
[28] A. Thorne, A. Kruth, D. Tunstall, J.T.S. Irvine, W.Z. Zhou, J. Phys. Chem. B 109 (12) (2005) 5439.
[29] D.L. Wilcox Sr., M. Berg, T. Bernat, D. Kelleman, J.K. Cochran Jr., Hollow and Solid Spheres and Microspheres: Science and Technology Associated with their Fabrication and Application, MRS Proc., vol. 372, Materials Research Society, Pittsburgh, PA, 1994.

[30] E. Mathlowitz, J.S. Jacob, Y.S. Jong, G.P. Carino, D.E. Chickering, P. Chaturvedl, C.A. Santos, K. Vijayaraghavan, S. Montgomery, M. Bassett, C. Morrell, Nature 386 (1997) 410.
[31] H. Huang, E.E. Remsen, J. Am. Chem. Soc. 121 (1999) 3805.
[32] Z.Z. Yang, Z.W. Niu, Y.F. Lu, Z.B. Hu, C.C. Han, Angew. Chem. Int. Ed. 42 (2003) 1943.
[33] R.F. Xu, X.X. Hu, W.K. Hu, P. Zhang, Abstr. Papers Amer. Chem. Soc. 226: U705-U705 213-Inor Part 1, Sep. 2003.
[34] D. Walsh, S. Mann, Nature 377 (1995) 320.
[35] A. Imhof, D.J. Pine, Nature 389 (1995) 948.
[36] J. Jang, J.H. Oh, Adv. Mater. 15 (2003) 977.
[37] S.C. Gu, T. Kondo, E. Mine, D. Nagao, Y. Kobayashi, M. Konno, J. Colloid Interface Sci. 279 (2004) 281.
[38] D. Walsh, J.D. Hopwood, S. Mann, Science 264 (1994) 1576.
[39] M. Ohmori, E. Matijevic, J. Colloid Interface Sci. 150 (1992) 594.
[40] S.D. Sims, D. Walsh, S. Mann, Adv. Mater. 10 (1998) 151.
[41] D.S. Bae, D.J. Kim, K.S. Han, J.H. Adair, J. Ceram. Proc. Res. 3 (2002) 38.
[42] C.W. Guo, Y. Cao, S.H. Xie, W.L. Dai, K.N. Fan, Chem. Commun. (2003) 700.
[43] S.S. Chan, I.E. Wachs, L.L. Murrell, J. Phys. Chem. 88 (1984) 5831.
[44] J.A. Horsley, I.E. Wachs, J.M. Brown, G.H. Via, F.D. Hardcastle, J. Phys. Chem. 91 (1987) 4014.
[45] C.D. Wagner, W.M. Riggs, L.E. Davis, J.F. Moudler, G.E. Muilenberg (Eds.), Handbook of X-Ray Photoelectron Spectroscopy, Perkin–Elmer, 1992, p. 73.
[46] J. Pouilleau, D. Devilliers, H. Groult, J. Mater. Sci. 32 (1997) 5645.
[47] S. Doniach, M. Sunjic, J. Phys. C 3 (1970) 285.
[48] F. Le Normand, J. El Fallah, L. Hilaire, P. Lègarè, A. Kotani, J.C. Parlebas, Solid State Commun. 71 (1989) 885.
[49] M. Valigi, D. Gazzoli, I. Pettiti, G. Mattei, S. Colonna, S. De Rossi, G. Ferraris, Appl. Catal. A 231 (2002) 159.
[50] A.F. Carley, G. Spoto, P.R. Chalker, J.C. Riviere, M.W. Roberts, J. Chem. Soc., Faraday Trans. I 83 (1987) 351.
[51] P.M. Kumar, S. Badrinarayanan, M. Sastry, Thin Solid Films 358 (2000) 122.
[52] B.M. Lok, B.K. Marcus, C.L. Angnell, Zeolites 6 (1986) 185.
[53] C. Martin, P. Malet, G. Solana, V. Rives, J. Phys. Chem. B 102 (1998) 2759.
[54] F. Somma, P. Canton, G. Strukul, J. Catal. 229 (2) (2005) 490.
[55] W. Janusz, A. Sworska, J. Szczypa, Colloids Surf. A 152 (1999) 223.